# Journal of Materials Chemistry A

Accepted Manuscript


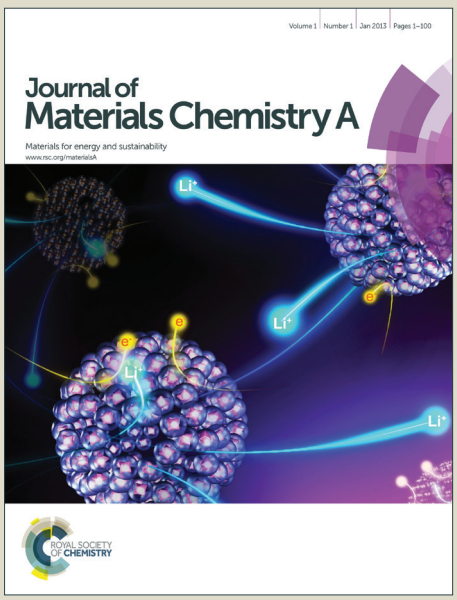





ROYAL SOCIETY OF CHEMISTRY

www.rsc.org/materialsA

Journal Name

RSCPublishing

ARTICLE

# A facile one-step hydrothermal synthesis of α-$Fe_2O_3$ nanoplates imbedded in graphene networks with high rate lithium storage and long cycle life

Cite this: DOI: 10.1039/x0xx00000x

Received 00th January xxx,
Accepted 00th January xxx

DOI: 10.1039/x0xx00000x

www.rsc.org/

Shuangke Liu *, Zhongxue Chen, Kai Xie, Yujie Li, Jing Xu and Chunman Zheng *

College of Aerospace Science and Engineering, National University of Defense Technology, Changsha, 410073, China. E-mail: liu_sk@139.com;zhengchunman@hotmail.com

In this study, we demonstrate a facile one-step hydrothermal strategy to build a nanostructure of α-$Fe_2O_3$ nanoplates imbedded in graphene networks, using water and glycerol as hydrothermal solvents. The graphene oxide was chemically reduced via $Fe^{2+}$ and glycerol, the obtained α-$Fe_2O_3$ nanoplates with a thickness of 20~30 nm and a side length of 100~300 nm are well wrapped by and tightly contact with the flexible conductive graphene networks. When used as the anode material for lithium ion batteries, the rGO/α-$Fe_2O_3$ nanoplate composite demonstrates high discharge capacities of ~896 $mAhg^{-1}$ till 200 cycles at 5C and ~429 $mAhg^{-1}$ up to 1000 cycles even at 10C rate. The excellent lithium storage performance could be attributed to the synergistic effects of the unique structures, which can provide fast electron transport and shorten the diffusion path of the Li ions as well as accommodate the volume change of the composite in the cycling.

## Introduction

An increasing demand for lithium ion batteries with high energy density, high power density and long cycle life has been present in recent years, due to the ever-rising concerns for electric vehicles (EVs) and grid storage of electricity produced by renewable energies[1,2]. However, graphite, the current commercialized anode materials of lithium-ion battery, has a relatively low theoretical specific capacity of 372 $mAhg^{-1}$[3]. Thus, it is necessary to develop alternative anode materials and novel nanostructures to meet the growing demands for lithium storage performance. α-$Fe_2O_3$ has been considered as one of the most promising candidate anode materials due to its high theoretical capacity, low cost, and nontoxicity[4-8].However, there remain some problems to be addressed for its practical application. The lithium storage mechanism of the α-$Fe_2O_3$ can be described as follows: $Fe_2O_3+6Li^++6e^-=2Fe+3Li_2O$.The α-$Fe_2O_3$ suffers from large volume expansion during cycling and low conductivity characteristics, which result in large capacity loss, poor cycling stability and rate performance[9-11].

To address these issues, tremendous efforts have been made during the past decades. One common strategy is to build unique nanostructures such as nanoparticle[12-14], hollow particle[15,16],hierarchical hollow structure[17,18], core-shell structure[19] ,nanotube[9,20], nanoflake[4], nanorod[21],nanodendrite[22], nanodisk[23,24]. These nanostructures provide a short transport path of Li ions and high active contact area, furthermore, the nanostructures could effectively buffer the stress induced during the charge-discharge process[25].Another strategy is to combine these α-$Fe_2O_3$ nanostructures with conductive carbon matrix such as carbon nanofibers[26], carbon nanotubes[27] and graphene[21,24,28-41].Particularly, graphene is considered as a promising two-dimensional conductive support for energy storage applications owing to its superior electronic conductivity, high chemical stability, remarkable structural flexibility and high theoretical specific surface area [42, 43]. Moreover, the graphene nanosheet itself can also be used as lithium-ion battery anodes which demonstrate higher reversible capacity compared to graphite [44]. In the past three years, combining α-$Fe_2O_3$ nanostructures with graphene-based materials have been reported to substantially enhance battery performance of the composites [21, 24, 28-41]. Among them, few nanostructures of graphene based nanoplate-like or nanosheet-like α-$Fe_2O_3$ anodes with excellent battery performance are reported, except that Jin et al [28] reported a $Fe_2O_3$-graphene sheet on sheet nanocomposite using a water-isopropanol solvothermal method. However, a reversible capacity of only 662.4 $mAhg^{-1}$ could be reached after 100 cycles at 1C rate. Despite of these progress, it is still a great challenge to fabricate graphene-based α-$Fe_2O_3$ nanostructures both with high rate lithium storage and long cycle life.

Herein, we report a facile one-step hydrothermal synthesis of α-$Fe_2O_3$ nanoplates imbedded in graphene networks, using water and glycerol as hydrothermal solvents. No additives of other metal ions, halogen ions or PVP, which are usually used in other reports when preparing nanoplate-like or nanosheet-like $Fe_2O_3$ [45], are needed in this system, escaping the generation of impurities. Moreover, the graphene oxide (GO) rather than thermally reduced graphene oxide (rGO) is introduced to the solvothermal reaction system. It is know

that the GO is easy to disperse in water and glycerol and full of functional groups to bond with $Fe_2O_3$ crystal. As expected, the resulting α-$Fe_2O_3$ nanoplates are well-imbedded in the reduced graphene oxide sheets, preventing the graphene sheets from restacking. At the same time, the graphene networks help to control the nucleation and growth of the α-$Fe_2O_3$ nanoplates. Such unique nanostructures demonstrate high reversible capacity as well as stable cycle performance at high rates with discharge capacities of 896 $mAhg^{-1}$ till 200 cycles and 429 $mAhg^{-1}$ up to 1000 cycles at 5C and 10C rate, respectively. To the best of our knowledge, there is no report on graphene-based α-$Fe_2O_3$ electrodes that can deliver such long cycle life with stable high rate performance till now. In addition, the synthesis approach presents a simple, tunable and environmentally friendly method for the large-scale synthesis of metal oxide/grapheme hybrid composite nanostructures.

## Results and discussion

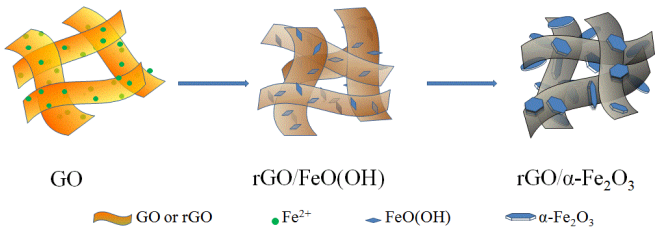


**Figure 1** Schematic illustration of the formation of rGO/α-$Fe_2O_3$ nanoplate composite

The synthetic route of the rGO/α-$Fe_2O_3$ nanoplate composite can be schematically illustrated in **Figure 1**. First, the $Fe^{2+}$ ions from $FeSO_4$ are favorably adsorbed on the surface of the well-dispersed GO sheets via electrostatic interactions [33]. Then when heating the hydrothermal system to a relatively low temperature, the $Fe^{2+}$ on the surface of the GO sheet hydrolyze, and the FeO(OH) heterogeneously nucleate at the interface to form ultrafine nanorice-like particles, the GO sheet is mildly co-reduced by the $Fe^{2+}$ and glycerol under the pressure-tight hydrothermal condition, resulting in the nanostructure of rGO/FeO(OH) (see Figure S1a).Upon heating the system to a higher temperature, the FeO(OH) transform into α-$Fe_2O_3$, which is also confirmed by a previous report [46]. With the presence of glycerol, the α-$Fe_2O_3$ nanoparticle assembles to nanoplate-shaped structures (see Figure S1b, S1c and S1d). During the hydrothermal heating process, the oxygen functional groups on the GO sheets are reduced to generate graphene networks, and the α-$Fe_2O_3$ nanoplates imbedded in the networks prevent from the restacking of the graphene sheets during hydrothermal and drying process (see Figure S3)**.** Because of the plentiful oxygen functional groups, the GO surface interacts strongly with the wrapped α-$Fe_2O_3$ nanoplates, hindering the growth of the crystalline.

It is noteworthy that the adding of glycerol as solvent plays a critical role in the formation process of these α-$Fe_2O_3$ nanoplates. When only water was added into the system, heterogeneous spherical particles with sizes ranging from 100~500 nm are formed (see Figure S4a, S4b). Some particles consist of densely packed smaller spherical subunits, some particles with smooth surface morphology have no subunits. However, when the GO solution was absent while the glycerol was added, smaller α-$Fe_2O_3$ nanoplates of 100~300 nm were obtained under the same hydrothermal conditions (see Figure S4c, S4d). This indicates without glycerol, FeO(OH) nanoparticles appreciably grow in the free solution instead of on graphene oxide sheets as a result of fast hydrolysis. The existence of glycerol may create a suitable reaction environment to help the adsorption of $Fe^{2+}$ on the surface of GO as well as slow down the hydrolysis of the $FeSO_4$, which lead to the generation of the nanoplate-like crystal. We also found that the glycerol content in the hydrothermal system presents important effect on the micro-morphology of the nanostructures (see Figure S5). It can be seen that when there is a trace amount of glycerol (Figure S5b), large α-$Fe_2O_3$ nanoplates with a thickness of ~100 nm and a side length of ~500 nm and smaller spherical particles emerge under the hydrothermal condition; when the glycerol increases to 20 ml (Figure S5c), smaller and thinner α-$Fe_2O_3$ nanoplates are loosely imbedded in the graphene networks and there is almost no spherical particles existing; when the glycerol increases to 40 ml (Figure S5d), much smaller α-$Fe_2O_3$ nanoplates are densely distributed among the graphene sheets. This indicates that the glycerol may slow down the hydrolysis of the $FeSO_4$ and prevent the α-$Fe_2O_3$ nanoplates from growing up. As the previous report [47] indicates, the FeO(OH) nanoplate crystal tend to be smaller while coating on graphene oxide than on graphene sheet due to the functional groups and defects on the GO surface. Thus the in-situ generation of α-$Fe_2O_3$ in GO solution may hinder the growth of the α-$Fe_2O_3$ nanoplates.

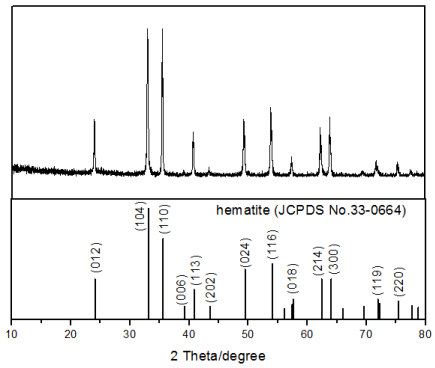


**Figure 2** XRD patterns of the rGO/α-$Fe_2O_3$ nanoplate composite

**Figure 2** shows the powder X-ray diffraction (XRD) patterns of the obtained composite, all diffraction peaks in the composite agree well with the standard card of α-$Fe_2O_3$ (JCPDS 33-0664). The diffraction angles of the composite are a little lower than that of the standard XRD patterns, indicating increased d-spacing of the composite according to the Bragg equation of $\lambda=2d\sin\theta$, which could be further confirmed by high resolution TEM images. The intensity of the (104) and (110) peaks are almost the same in the composite while the intensity of the (104) peak is stronger than that of the (110) peak in the standard patterns. This may be ascribed to a trace amount of γ-Fe2O3 (JCPDS No.39-1346) existing in the composite, the overlap of (110) peak at 35.61° for α-$Fe_2O_3$ and (119) peak at 35.65° for γ-$Fe_2O_3$ resulted in an intensified peak at ~35.65° [48]. The sharp peaks indicate the good crystallinity of the α-$Fe_2O_3$ in the composite. Generally, good crystallinity of the electrode material helps to enhance the transport of lithium ions in the crystal. It is noted that the hydrothermal reaction temperature plays an important role on the crystal structure of the composite (see Figure S2). When the temperature is below 120 ℃, the XRD pattern of as obtained composite agrees well with goethite FeO(OH) with broad peaks, indicating low crystallinity of the composite. When the temperature was increased above 120℃ (140℃, 160℃, 180℃), the XRD patterns can be indexed to hematite α-$Fe_2O_3$, and the intensity of the diffraction peaks become stronger as the heating temperature increases. Figure

S2 presents the transition temperature of 120~140℃ from goethite FeO(OH) to hematite α-$Fe_2O_3$ under the hydrothermal condition in this study.

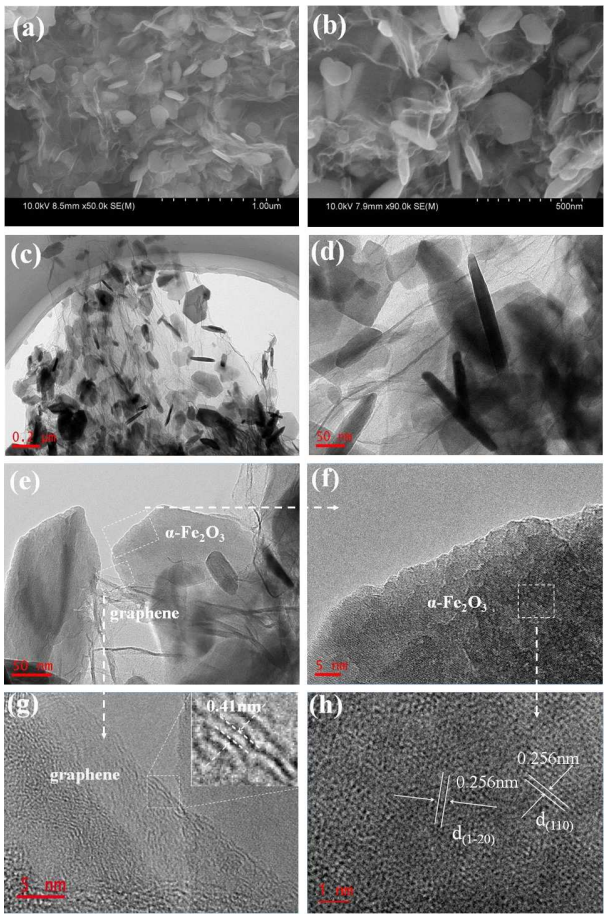


**Figure 3** SEM (a,b) and TEM (c,d,e) images of the rGO/α-$Fe_2O_3$ nanoplate composite

**Figure 3** shows the scanning electron microscopy (SEM) and transmission electron microscopy (TEM) images of the rGO/α-$Fe_2O_3$ nanoplate composite. Figure 3a, 3b reveals that α-$Fe_2O_3$ nanoplates are uniformly wrapped by curled graphene nanosheets with anisotropic orientation of the nanoplates. Typically, the α-$Fe_2O_3$ shows irregular plate-like morphology with a thickness of 20~30 nm and a side length of 100~300 nm, which could be confirmed both by SEM (Figure 3b) and TEM (Figure 3d) images. The nanoscale sizes (thickness 20~30 nm, length 100-300 nm) of the α-$Fe_2O_3$ nanoplate were desirable owing to decreased transport length for Li ions and electrons. Figure 3d further confirms that the α-$Fe_2O_3$ nanoplate was an intact crystalline rather than composed of layered disks or sheets which is reported previously [24]. Figure 3d shows the typical interface between the rGO and α-$Fe_2O_3$ nanoplate, the high-resolution TEM images of the α-$Fe_2O_3$ nanoplate lying horizontally in Figure 3f could further reveal the crystal growth orientation, and the lattice distances of 0.256 nm with two different orientations in figure 3h are corresponding to (110) and (1-20) planes of α-$Fe_2O_3$, respectively. This shows the selectively oriented growth of α-$Fe_2O_3$ is perpendicular to the (001) plane. The folded structure of the graphene edge in figure 3g allows for the evaluation about the thickness and interlayer spacing, indicating an interlayer distance of 0.41nm and a triple-layer of the graphene. It is noted that the TEM images were obtained after vigorous sonication for 2h, the α-$Fe_2O_3$ nanoplates are still tightly attached to the graphene networks, indicating strong bond between the α-$Fe_2O_3$ nanoplates and graphene. The α-$Fe_2O_3$ nanoplates are wrapped within the ultrathin and flexible graphene networks, which can effectively prevent the aggregation of α-$Fe_2O_3$ nanoplates as well as accommodate the volume change during long cycles of charge and discharge. In addition, the conductive graphene networks with direct and tight contact of α-$Fe_2O_3$ nanoplates could provide an efficient lithium ion and electron transport for the electrochemistry process of α-$Fe_2O_3$ nanoplates.

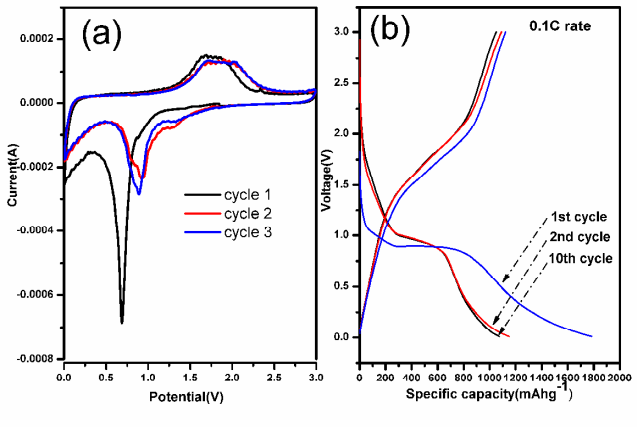


**Figure 4** CV (a) and charge-discharge (b) curves of the rGO/α-$Fe_2O_3$ nanoplate composite

The electrochemical property of the rGO/α-$Fe_2O_3$ nanoplate composite was systematically investigated at room temperature. **Figure 4**a shows the representative cyclic voltammograms (CVs) of the rGO/α-$Fe_2O_3$ nanoplate composite. There is a sharp cathodic peak observed at 0.7V at the first cycle for the composite, representing the Li insertion into the α-$Fe_2O_3$ and the formation of amorphous $Li_2O$, which have been well elaborated in previous studies [4, 9, 18, 49]. This cathodic peak is obviously higher than that of previous reports [18, 49], indicating easier Li insertion reaction for the rGO/α-$Fe_2O_3$ nanoplate composite. The reduction peak of 0.7V shifts to a higher potential of 0.9V at subsequent cycles, indicating the irreversible phase conversion in the first cycle [31]. On the other hand, a broad oxidation peak of 1.6~1.9 V, which could be attributable to the oxidation from $Fe^0$ to $Fe^{2+}$ and $Fe^{2+}$ to $Fe^{3+}$, are found in following anodic process. For the second sweep cycle, a cathodic peak at 1.3V appeared after the first cycle, which is attributed to the conversion of α-$Fe_2O_3$ to the cubic $Li_2Fe_2O_3$, indicates the activation process of the first cycle [4]. It is noteworthy that after the first cycle, the CV peaks overlap well, indicating good reversibility of the discharge–charge reactions of the composite.

Figure 4b shows the charge-discharge voltage profiles of the rGO/α-$Fe_2O_3$ nanoplate composite at 0.1C rate (1C=1000mA$g^{-1}$). It's noted that the rGO displays high capacities as anode materials, as figure S7 shows, the rGO prepared under water-glycerol hydrothermal conditions have discharge and charge capacities of 1521.5 and 584.2 mA$hg^{-1}$, respectively. The rGO in the composite also contributes capacities during charge and discharge process, so the specific capacities are calculated based on the total mass of the rGO/α-$Fe_2O_3$ nanoplate composite in this article. The initial discharge and charge capacities are 1782.9 and 1121.8 mAh $g^{-1}$, respectively (the values are 1248 and 785.3 mA$hg^{-1}$, respectively, based on the mass of α-$Fe_2O_3$ suppose the rGO has equal specific capacity as α-$Fe_2O_3$). The composite has a low coulombic efficiency of 62.9%, the irreversible

capacity loss in the first cycle is most likely due to incomplete reversible reaction and inevitable formation of solid electrolyte interface (SEI) of the composite [50]. However, the coulombic efficiency rises rapidly to 93.5% in the second cycle and reaches 97.9% in the 10th cycle, suggesting an excellent reversible $Li^+$ intercalation/extraction performance.

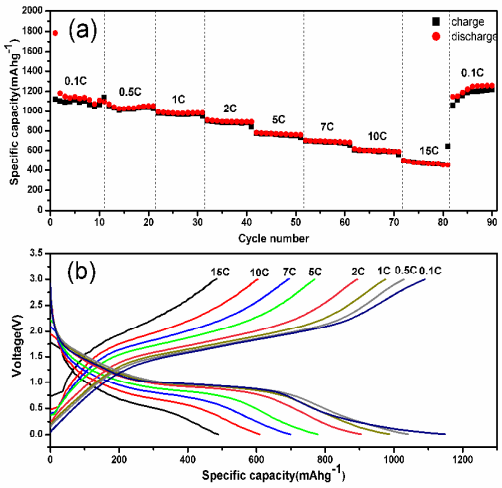


**Figure 5** the cycling capacities (a) and charge-discharge curves (b) of the rGO/α-$Fe_2O_3$ nanoplate composite at various C rates

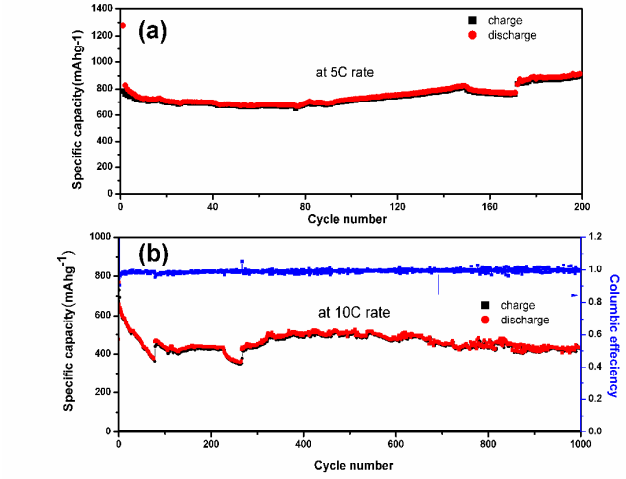


**Figure 6** the cycling performance of the rGO/α-$Fe_2O_3$ nanoplate composite at 5C and 10C rate (identical charge and discharge rate)

In order to evaluate the rate performance of the electrodes, the discharge−charge tests were carried out at various current densities. **Figure** 5a and figure 5b show the cycling capacities and the discharge−charge curves of the electrode at different C rates, respectively. Stable reversible capacities of 1149, 1041, 986.5 and 899.4 $mAhg^{-1}$ were retained at 0.1C, 0.5C, 1C and 2C rates, respectively. Remarkably, stable reversible capacities of ~774, ~697, ~603 and ~475 $mAhg^{-1}$ could still be delivered when the C rates rise to 5C, 7C, 10C and 15C, respectively, indicating the rGO/α-$Fe_2O_3$ nanoplate composite has excellent rate performance. When the C rate reduces back from 15C to 0.1C, the discharge capacity could still reach ~1253 $mAhg^{-1}$, indicating excellent reversibility of the composite. Moreover, the discharge capacity rises slowly with the cycle number, the reason for this observation will be discussed in following paragraph. As a comparison, the rGO/α-$Fe_2O_3$ hybrid and the α-$Fe_2O_3$ nanoplate prepared without adding of glycerol and graphene oxide respectively show much poorer rate performance (see figure S8a). The outstanding rate performance of the rGO/α-$Fe_2O_3$ nanoplate composite should be attributed to the synergistic effects of the well dispersed α-$Fe_2O_3$ nanoplates and conductive flexible graphene networks. Recently, Lu et al [51]found that α-$Fe_2O_3$ nanoplates exhibit significantly improved electrochemical performance compared with α-$Fe_2O_3$ nanograins, it is suggested the α-$Fe_2O_3$ nanoplates have hexagonal framework with pores on the (001) basal surfaces, readily supplying a pathway for easy lithiation-delithiation, and the shorter thickness along the <001> direction provide shorter transport length for $Li^+$ and electrons. At the same time, the conductive graphene networks with direct and tight contact of α-$Fe_2O_3$ nanoplates also provide fast lithium ion and electron transport for the composite, which will greatly enhance the rate performance of the composite.

To test the long cycle stability of the rGO/α-$Fe_2O_3$ nanoplate electrodes, the discharge−charge measurements were carried out at 5C and 10C rates, respectively. Figure 6a, 6b shows the extremely high cyclic stability of the electrode at such high C rates. As is shown, a capacity of 896 mAh $g^{-1}$ is still retained till 200 cycles at 5C. Except for the large capacity loss for the first cycle, the capacity of the composite electrode shows a slow decrease from 828 $mAhg^{-1}$ in the second cycle to 666.4 $mAhg^{-1}$ in the 77th cycle, followed by slow increase in the subsequent steps as mentioned above. Similar phenomena have also been observed in previous reports [18, 25, 52]. The slight capacity fade should be attributed to the pulverization of the α-$Fe_2O_3$ nanoplates during the initial cycles, resulting in the loss of the electrical connectivity between the particles and current collector. The subsequent capacity increase may be explained as follows: 1) the pulverized nanoplates are attached to the graphene networks during subsequent cycles, which will facilitate the reversible reaction of the electrode, 2) the graphene networks itself contributes to part of the reversible capacity as figure S7 shows. As a comparison, figure S5b shows the cycling performance of the rGO/α-$Fe_2O_3$ hybrid and the α-$Fe_2O_3$ nanoplate at 5C rate. The rGO/α-$Fe_2O_3$ hybrid delivers low but relatively stable cycling capacities compared with the rGO/α-$Fe_2O_3$ nanoplates, indicating the nanoplate shape of α-$Fe_2O_3$ is favourable to the lithium storage and conversion than the nanoparticle shape. The α-$Fe_2O_3$ nanoplate undergoes rapid capacity fade during the initial cycles compared with the rGO/α-$Fe_2O_3$ nanoplates, indicating the graphene networks in the composite play a key role in the excellent long cycling performance as well as high rate capacity as explained above. The synergistic effects of the α-$Fe_2O_3$ nanoplates and graphene networks result in the superior electrochemical performance of the rGO/α-$Fe_2O_3$ nanoplate composite.

Noticeably, the electrode delivers a capacity of 429 mAh $g^{-1}$ at 10 C rate up to 1000 cycles with high coulombic efficiency of ~99%, as show in figure 6b. To the best of our knowledge, such high capacity with ultralong cycle life at 10 C rate in our rGO/α-$Fe_2O_3$ nanoplate composite as anode have not been reported before. Table 1 shows the cycling performance of α-$Fe_2O_3$ nanostructures reported in recent years, our rGO/α-$Fe_2O_3$ nanoplate nanostructures show superior performance than the others. This outstanding performance could be attributed to the unique nanostructure of the composite in which thin nanoplate with stacked (001) planes effectively shorten the diffusion path of Li ions, and the flexible conductive graphene networks provide fast electron transport and effectively guarantee the structural stability during the charge-discharge process. Additionally, the high surface area derived from the thin graphene and α-$Fe_2O_3$ nanoplate provides efficient contact area of the electrolyte/active materials.

**Table 1.** The cycling performance of some α-$Fe_2O_3$ nanostructures reported in recent years

| Ref. | $Fe_2O_3$ anode | Carbon content/wt% | Cycling performancem/$Ahg^{-1}$ |
|---|---|---|---|
| This work | rGO/α-$Fe_2O_3$ nanoplate | 30 graphene<br>10 carbon SP | 896/5C/200 cycles<br>429/10C/1000 cycles |
| 24 | α-$Fe_2O_3$/RGO | 24.4 RGO<br>20 carbon SP | ~337/10C/150 cycles<br>~516 /3C/150 cycles |
| 29 | $Fe_2O_3$/graphene rice on sheet | 52.6 graphene<br>10 acetylene black | ~800/0.2C/100 cycles |
| 30 | RGO-$Fe_2O_3$ nanospindle | 24.4 RGO<br>10 acetylene black | 336/5C /100 cycles |
| 28 | $Fe_2O_3$-graphene sheet-on-sheet | 59.4 graphene<br>10 acetylene black | 622.4/1C /100 cycles<br>322.5/5C/ 100 cycles |
| 32 | RGO/ $Fe_2O_3$ | 20 RGO | 1027/ 0.1C /50 cycles |
| 33 | $Fe_2O_3$/Graphene Aerogel | 22 graphene<br>10 Carbon SP | 372/5C/50 cycles |
| 34 | $Fe_2O_3$/graphene nanocomposite | — Graphene<br>10 acetylene black | 220/ 3C/30 cycles |
| 27 | G-CNT-Fe 3Dnanostructure | — Graphene/CNT<br>15 ketjen black | ~865/ 0.1C/45 cycles |
| 17 | α-$Fe_2O_3$ hollow spheres | 10 Super-P | 710/ 0.2C/100 cycles |
| 19 | Hierarchical core–shell α-$Fe_2O_3$@C nanotube | 20 carbon black | 482/4C/ 1000 cycles |
| 53 | $Fe_2O_3$/GS Aerogel | 45.9 graphene<br>10 carbon black | 733/2C/ 1000 cycles |
| 18 | Hierarchical hollow spheres of α-$Fe_2O_3$ nanosheet | 10 acetylene black | 815/ 0.5C/200 cycles |

## Experimental

**Synthesis of Graphite Oxide**. Graphite oxide was synthesized from natural graphite by an improved Hummers method [54]. Briefly, a 9:1 mixture of concentrated $H_2SO_4$/$H_3PO_4$ (120:14 ml) was added to a mixture of graphite powders (1.0 g) and $KMnO_4$ (6.0 g) under magnetic stirring. The reaction was then heated to 50 °C and stirred for 12 h. The reaction was cooled to room temperature and poured onto ice (140 ml), then 60ml 30% $H_2O_2$ was poured to the mixture until it turns to gold yellow. After that, the yellow solution was centrifuged and washed in succession with 200 ml of water, 300 ml of 10% HCl, and 900 ml of ethanol to remove other ions. The solid obtained after centrifuged was vacuum-dried for 24h at room temperature.

**Preparation of rGO/α-$Fe_2O_3$ nanoplate.** The rGO/α-$Fe_2O_3$ nanoplate composite was prepared by a simple one-step hydrothermal method. First, 1.1g $FeSO_4 \cdot 7H_2O$ (99% purity, Tianjin Damao chemical Reagent Co., Ltd) were dissolved in water-glycerol alcohol solution (80ml water and 20ml glycerol), and then 0.04g graphite oxide was added into 40ml water and sonicated for 2h to obtain the graphene oxide solution. Subsequently the two as-prepared solutions were mixed together with continuous stirring for 30min. The mixed solution was sealed into 200 ml Teflonlined stainless steel autoclave and heat treated at 140~180 °C for 10 h. The as-prepared products were collected by filtration, washed with water and ethanol for several times, and dried at 80°C for 10h.

**Materials Characterizations.** The structure of rGO/α-$Fe_2O_3$ nanoplate composites were measured by XRD (SIEMENS D-500) using Cu Kα radiation, ranging from 10° to 80° at a step of 8 °·$min^{-1}$. The micro morphologies of the composites were studied using field emission scanning electron microscopy (HITACHI S4800, Japan) and transmission electron microscopy (TEM, TECNAI, Philips, Netherlands). The thermogravimetric analysis (TGA) was measured with a TGA-600 with a heating rate of 10°·$min^{-1}$ to determine the graphene content in the composite. It contained 30 wt % rGO as measured by TGA (see Figure S3).

**Electrochemical Characterization.** Electrochemical experiments were performed using 2016 coin-type cells. The working electrode of the rGO/α-$Fe_2O_3$ nanoplate composite was prepared by mixing 80 wt% active material (rGO/α-$Fe_2O_3$ nanoplate composite) with 10 wt% Super P and 10 wt% polyvinylidene fluoride (PVDF) binder using N-methyl-pyrrolidone (NMP) as the solvent. After mixing well, the slurry was pasted on copper foil and dried overnight at 100°C in a vacuum oven.. The metallic lithium foils and 1 M $LiPF_6$ in EC/DEC (1:1 by volume) were used as the counter electrode and electrolyte, respectively, and Celgard 2400 was the separator. Galvanstatic charge-discharge measurements were performed using a battery tester (LAND CT-2001A, Wuhan, China) at room temperature in a potential range of 0.01~3.0 V (*vs.* $Li^+$/Li) at various current densities. The specific capacity was calculated based on the mass of the rGO/α-$Fe_2O_3$ nanoplate composite. The areal loading density of the composite in the copper is 0.3~0.5 mg $cm^{-2}$.Cyclic voltammetry (0.01~3.0 V, 0.1 mV $s^{-1}$) was performed with an electrochemical workstation (CHI 660C).

## Conclusions

In conclusion, we have demonstrated a facile one-step hydrothermal strategy to build a nanostructure of α-$Fe_2O_3$ nanoplates imbedded in graphene networks. In this method, the graphene oxide can be effectively co-reduced by $Fe^{2+}$ and glycerol, the thin α-$Fe_2O_3$ nanoplates were well dispersed in the graphene networks with tight contact. The unique structures can provide fast electron transport and shorten the diffusion path of the Li ions as well as accommodate the volume change of the composite in the cycling, leading to superior lithium storage and long cycle life. The rGO/α-$Fe_2O_3$ nanoplate composite demonstrates high discharge capacities of ~896 $mAhg^{-1}$ till 200 cycles at 5C and ~429 $mAhg^{-1}$ up to 1000 cycles even at 10C rates. In addition, the simple, tunable and environmentally friendly synthesis approach described in this work can be extended to the large-scale fabrication of metal oxide/graphene hybrid composite nanostructures.

## Acknowledgements
We are appreciating to the Aid Program for Science and Technology Innovative Research Team in Higher Educational

Institutions of Hunan Province and the Hunan Provincial Natural Science Foundation of China (No. 13JJ4004).

## Notes and references

Electronic Supplementary Information (ESI) available: [details of any supplementary information available should be included here]. See DOI: 10.1039/b000000x/

1 M. Armand.,J. M. Tarascon, *Nature* **2008**, 451, 652.

2 B. Kang, G. Ceder, *Nature* **2009**, 458, 190.

3 H. Buqa,D. Goers, M. Holzapfel, M. E.Spahr, P. Novak, *J. Electrochem. Soc.* **2005**, 152, A474.

4 M. V. Reddy, T. Yu, C. H. Sow, Z. X. Shen, C. T. Lim, G. V. S. Rao, B. V. R. Chowdari, *Adv. Funct. Mater.* **2007**, 17, 2792.

5 D. Larcher, C. Masquelier, D. Bonnin, Y. Chabre, V. Masson, J. B. Leriche, J. M. Tarascon, *J. Electrochem. Soc.* **2003**, 150, A133.

6 B. Koo, H. Xiong, M. D. Slater, V. B. Prakapenka, M. Balasubramanian, P. Podsiadlo, C. S. Johnson, T. Rajh, E. V. Shevchenko, *Nano Lett.* **2012**, 12,2429.

7 L. Zhang, H. B. Wu, S. Madhavi, H. H. Hng, X. W. Lou, *J. Am. Chem. Soc.* **2012**, 134,17388.

8 J. S. Xu, Y. J. Zhu, *ACS Appl. Mater. Interfaces* **2012**, 4, 4752.

9 J. Chen, L. N. Xu, W. Y. Li, X. L. Guo, *Adv. Mater.* **2005**,17, 582.

10 X.L. Wu, Y.G. Guo, L.J. Wan, C.W. Hu , *J Phys Chem C* **2008**,112,16824.

11 H. Liu, G. Wang, J. Park, *Electrochim Acta* **2009,**54,1733.

12 Y.N. NuLi, R. Zeng, P. Zhang, Z.P. Guo, H.K. Liu, *J Power Sources* **2008**, 184, 456.

13 J.M. Ma, J. B. Lian, X. C. Duan, X. D. Liu, W. J. Zheng, *J. Phys. Chem. C* **2010**,114, 10671.

14 M. F. Hassan, M. M. Rahmana, Z. P. Guo, Z. X. Chen, H. K.. Liu, *Electrochim. Acta* **2010**,5,5006.

15 H. S. Kim, Y. Piao, S. H. Kang, T. Hyeon, Y. E. Sung, *Electrochem. Commun.* **2010**, 12, 382.

16 J. S. Zhou, H. H. Song, X. H. Chen, L. J. Zhi, S. Y. Yang, J. P. Huo, W. T.Yang, *Chem. Mater.* **2009**, 21, 2935.

17 B. Wang, J. S. Chen, H. B. Wu, Z.Y. Wang, X.W. Lou. *J. Am. Chem. Soc.* **2011**, 133, 17146.

18 J.X. Zhu, Z.Y. Yin, D. Yang, T. Sun, H.Yu, H. E. Hoster,H. H. Hng, H. Zhang ,Q.Y. Yan, *Energy Environ. Sci.* **2013**, 6, 987.

19 X. Gu, L. Chen, S. Liu, H.Y. Xu, J. Yang, Y.T. Qian, *J. Mater. Chem. A* **2014**, 2, 3439.

20 Z.Y. Wang, D.Y. Luan, S. Madhavi, C.M. Li, X.W. Lou, *Chem.Commun.* **2011**, 47, 8061.

21 B.Zhao, R.Z. Liu, X.H. Cai, Z. Jiao, M.H. Wu, X.T. Ling, B. Lu, Y. Jiang, *J Appl. Electrochem.* **2014**, 44,53.

22 Q.T. Pan, K. Huang, S.B. Ni, F. Yang, S.M. Lin, D.Y. He, *J. Phys. D-Appl. Phys.* **2009** 42, 015417.

23 J. S. Chen,T. Zhu, X. H.Yang, H. G.Yang, X. W. Lou, *J. Am. Chem. Soc.***2010**,132,13162.

24 J. Qu, Y.X. Yin , Y.Q. Wang, Y. Yan, Y.G. Guo , W.G. Song, *ACS Appl. Mater. Inter.* **2013**,5, 3932.

25 J .S. Luo,J.L. Liu,Z.Y. Zeng,C.F. Ni,L.J. Ma,H. Zhang,J.Y. Lin, Z.X. Shen, H.J. Fan, ***Nano Lett.*** **2013**, 13, 6136.

26 L.W. Ji,O. Toprakci, M. Alcoutlabi,Y.F. Yao, Y. Li, S. Zhang, B.K. Guo, Z. Lin, X.W. Zhang, *ACS Appl. Mater. Interfaces* **2012**, 4, 2672.

27 S.H. Lee, V. Sridhar,J.H. Jung,K. Karthikeyan,Y.S. Lee,R. Mukherjee, N. Koratkar, I.K. Oh, *ACS nano*.**2013**,5,4242.

28 J. Kan , Y. Wang, *Sci. Rep.* **2013**,3.DOI: 10.1038/srep03502.

29 Y. Q. Zou, J. Kan, Y. Wang, *J. Phys. Chem. C* **2011**,115, 20747.

30 S. Bai ,S. Q. Chen, X. P. Shen, G. X. Zhua, G. X. Wang, *RSC Adv.* **2012**,2, 10977.

31 W. Xiao, Z.X. Wang, H.J. Guo, X.H. Li, J.X.Wang, S.L. Huang, L. Gan, *Appl. Surf. Sci.* **2013**, 266,148.

32 X. J. Zhu , Y. W. Zhu, S. T. Murali, M. D. Stoller, R. S. Ruoff, *ACS Nano***2011**, 5, 3333.

33 L. Xiao, D.Q. Wu, S. Han, Y.S. Huang, S. Li, M.Z. He , F. Zhang, X.L. Feng , *ACS Appl. Mater. Inter.* 2013, 5, 3764.

34 X. Y. Xue, C. H. Ma, C. X. Cui, L. L. Xing, *Solid State Sci.* **2011**,13, 1526.

35 S. Y. Liu, J.Xie, Q. Pan, C. Y.Wu , G. S. Cao, T. J. Zhu, X. B. Zhao, *Int. J. Electrochem. Sci.* **2012,**7, 354.

36 M. Zhang, B.H. Qu,D.N. Lei, Y.J. Chen, X.Z. Yu, L.B. Chen, Q.H. Li, Y.G. Wang, T.H. Wang, *J. Mater. Chem.* **2012**,22, 3868.

37 D. Z. Chen, W. Wei, R. N.Wang, J. C. Zhu, L. Guo, *New J. Chem.* **2012** 36, 1589.

38 L. Tian, Q. Zhuang, J. Li, C. Wu, Y. Shi, S. Sun, *Electrochim. Acta* **2012**,65, 153.

39 G.W. Zhou, J.L. Wang, P.F. Gao ,X.W. Yang , Y.S. He, X.Z. Liao,J. Yang , Z.F. Ma ,*Ind. Eng. Chem. Res.* **2013**,52, 1197.

40 M. Du, C. H. Xu, J. Sun, L. Gao, *J. Mater. Chem. A* **2013**,1, 7154.

41 S.H. Yu , D. E. Conte , S. Baek , D.C. Lee , S.K. Park , K. J. Lee , Y.Z. Piao , Y.E. Sung , N. Pinna, *Adv. Funct. Mater.* **2013**, 23, 4293.

42 N. Li, Z. Chen, W. Ren, F. Li, H.M. Cheng, *Proc. Natl. Acad. Sci.* **2012**, 109, 17360.

43 Z.X. Chen, M. Zhou, Y.L. Cao,X.P. Ai, H.X. Yang , J. Liu , *Adv. Energy Mater.* **2012**, 2,95.

44 X.F. Li, Y.H. Hu, J. Liu, A. Lushington, R.Y. Li ,X.L. Sun, *Nanoscale* **2013**, 5, 12607.

45 R.M. Liu, Y.W. Jiang, Q.Y. Lu,W. Du , F. Gao. *CrystEngComm* **2013**, 15, 443.

46 S.H. Yang, X.F. Song, P. Zhang, J. Sun, L. Gao. DOI: 10.1002/smll.201303922.



 

47 H.L. Wang, J. T. Robinson, G. Diankov, H.J. Dai. *J. Am. Chem. Soc.* **2010**, *132*, 3270.

48 Z.H. Wei, R.G. Xing, X. Zhang,S. Liu, H.H. Yu, P.C. Li, *ACS Appl. Mater. Interfaces* **2013**, 5, 598.

49 M.Du, C.H. Xu, J. Sun, L. Gao, *J. Mater. Chem. A*, **2013**, 1, 7154.

50 Q.M. Su, D. Xie,J. Zhang,G.H. Du, B.S. Xu. *ACS nano* **2013**, 7,9115. '

51 F.Q. Lu, Q.L. Wu, X.F. Yang, L.Q. Chen, J.J. Cai, C.L. Liang, M.M. Wu,P.K. Shen, *Phys.Chem. Chem. Phys.***2013**,15, 9768.

52 X. Zhang, H.X. Chen, Y.P. Xie, J.X. Guo, *J. Mater. Chem. A*, **2014**, 2,3912.

53 R.H. Wang , C.H. Xu , M. Du , J. Sun ,L. Gao , P. Zhang ,H.L. Yao , C.C. Lin, *Small* **2014**, DOI: 10.1002/smll.201303371.

54 D. C. Marcano, D. V. Kosynkin, J. M. Berlin, A. Sinitskii , Z.Z. Sun, A. Slesarev, L. B. Alemany, W. Lu, J. M. Tour, *ACS Nano* **2010**, 4,4806.